Computers and Electronics in Agriculture 211 (2023) 108029

Contents lists available at ScienceDirect

Computers and Electronics in Agriculture

journal homepage: www.elsevier.com/locate/compag

Quantifying effect of maize tassels on LAI estimation based on multispectral imagery and machine learning methods

Mingchao Shao [a,b,c,1], Chenwei Nie [a,b,c,1], Aijun Zhang [d,1], Liangsheng Shi [a], Yuanyuan Zha [a], Honggen Xu [c], Hongye Yang [c], Xun Yu [b,c], Yi Bai [b,c], Shuaibing Liu [b,c], Minghan Cheng [b,c], Tao Lin [e], Ningbo Cui [f], Wenbin Wu [g,*], Xiuliang Jin [a,b,c,*]

[a] State Key Laboratory of Water Resources and Hydropower Engineering Science, Wuhan University, Wuhan 430072, China
[b] National Nanfan Research Institute (Sanya), Chinese Academy of Agricultural Sciences, 572024 Sanya, China
[c] Institute of Crop Sciences, Chinese Academy of Agricultural Sciences, Key Laboratory of Crop Physiology and Ecology, Ministry of Agriculture, Beijing 100081, China
[d] National Engineering Research Center for Agriculture Northern Mountainous Areas, Agricultural University of Hebei, Baoding, Hebei 071000, China
[e] Institute of Cash Crops Research, Xinjiang Academy of Agricultural Sciences, Urumqi 830091, China
[f] Laboratory of Hydraulics and Mountain River Engineering & College of Water Resource and Hydropower, Sichuan University, 610065 Chengdu, China
[g] Institute of Agricultural Resources and Regional Planning, Chinese Academy of Agricultural Sciences, 100081 Beijing, China

ARTICLE INFO

Keywords:
Maize tassels
Segmentation
LAI
Vegetation indices

ABSTRACT

A reliable method to estimate the leaf area index (LAI) in a field environment is crucial for precise monitoring of crop-growth status. Currently, the crop canopy information has been widely used to estimate LAI using remote sensing methods. Many studies regard canopy tassels and leaves as integrated objects, no systematic study has yet investigated how tassels affect the accuracy of LAI estimates. Moreover, the estimation accuracy and generalization ability of the number of selected vegetation indices was seldom evaluated. Therefore, this study used deep learning segmentation methods to quantify how maize tassels affect LAI estimates and to evaluate how the number of variables affects LAI estimates. The results showed that the multispectral dataset segmentation tassels had the highest accuracy when using the VGG-encoded U-Net model (class pixel accuracy, CPA = 89.53 %; mean intersection over union, MIoU = 85.97 %). The segmentation accuracy first was increased and then decreased with tassel growth. By quantifying the contribution of tassels to the vegetation index, tassels most strongly affect the modified nonlinear vegetation index (MNLI) constructed from the canopy spectral information. Moreover, removing the tassels in images could significantly improve the accuracy of LAI estimates using the gradient-boosting decision tree method (GBDT). The estimation method obtained the highest accuracy when using nine vegetation indices to estimate the LAI (R^2 = 0.816, RMSE = 0.399, rRMSE = 7.4 %). Overall, the proposed method improves the accuracy of LAI estimates, which provides crucial technical support for monitoring the LAI of maize.

1. Introduction

Maize (*Zea mays*), a very important source of food and feed, is one of the most widely distributed food crops in the world (Andrimont et al., 2020). It is of strategic importance at the national level and has a high economic impact on agricultural producers. Accurately monitoring maize growth provides information that is essential for food security and for the economic security of farmers.

The leaf area index (LAI) is the ratio of the one-sided surface area of all green leaves to the surface area per unit of land (Breda, 2003; Liu et al., 2021). The LAI is a key parameter reflecting the crop-growth status, which gives information on the vegetation canopy structure and related material and energy-exchange processes (Morel et al., 2014; Putzenlechner et al., 2019). For instance, the information about LAI may be used to estimate dry matter content and crop yield (Dimitrov et al., 2019). Unfortunately, the LAI is traditionally measured in the field using hand-held testers, which is an accurate but labor-intensive method that is not operationally feasible for large-area field measurements (Lv et al.,

* Corresponding authors at: State Key Laboratory of Water Resources and Hydropower Engineering Science, Wuhan University, Wuhan 430072, China (X.J.).
E-mail addresses: wuwenbin@caas.cn (W. Wu), jinxiuliang@caas.cn (X. Jin).
[1] Mingchao Shao, Chenwei Nie and Aijun Zhang contributed equally.

https://doi.org/10.1016/j.compag.2023.108029
Received 22 February 2023; Received in revised form 9 June 2023; Accepted 11 June 2023
Available online 13 July 2023

2021). Therefore, a method for rapid, large-scale acquisition and analysis of the LAI is highly desirable.

The vegetation indices (VIs), a spectral transformation of two or more spectral bands, provides quantitative information on vegetation growth information on the ground monitored by remote sensing, which effectively and non-destructively describes green plant growth and biomass information (Jin et al., 2020a; Liang et al., 2015; Nguy-Robertson et al., 2014). The empirical model for estimating the LAI based on vegetation indices obtained from remotely sensed data was simple and thus widely studied. The study of Tanaka et al. (2015) has shown a strong linear relationship between LAI and the spectral index (SI) based on the difference between vegetation reflectance values at 760 nm and 739 nm. Kimma et al. (2020) used the Green Wide Dynamic Range Vegetation Index (GrWDRVI) obtained from STAIR fusion data and CubeSat data to build 2nd-order polynomial function model that accurately estimated the LAI of Corn [$R^2 = 0.75$, root mean square error (RMSE) = 1.10 ($m^2\ m^{-2}$)]. However, previous studies indicated that, for high-density vegetation, the saturation of optical remote-sensing imagery degraded the performance of these models for estimating biophysical parameters such as the leaf-area index (LAI), the FAPAR, and aboveground biomass(Cao et al., 2017; Haboudane et al., 2004; Liang et al., 2015; Nguy-Robertson et al., 2014). To enhanced the sensitivity to LAI estimation, Liang et al. (2015) build hybrid inversion models for LAI estimation and the optimized soil-adjusted vegetation index (OSVAI) and modified triangular vegetation index (MTVI2) estimated LAI with better accuracy (R^2 = 0.928, RMSE = 0.485). Nonetheless previous studies have estimated the LAI without considering the background (e.g., weeds, soil). For maize, the tassels are a non-photosynthetic vegetative component, and Bai et al. (2019) found that, reflectance in the visible bands increases on the canopy scale after removal tassels. Current studies calculated VIs by considering the tassels and the leaves as single integrated objects, but how the tassels affect the VI is not discussed. In addition, a single VI does not adequately reflect all crop-growth information, most studies have used more VIs to estimate LAI. Hence, it is crucial in estimation of LAI to reduce the interference of background factors and to select the appropriate number of VIs.

The current studies on tassels mostly involve destructive sampling (Dimitrov et al., 2019; Tan et al., 2013), and deep learning methods have been widely used as nondestructive methods for detection tassels. For example, Lu et al. (2016) proposed a region generation proposal based on graph partitioning algorithms and simple linear iterative clustering (SLIC), which combined an ensemble neural network to segment tassels with an average precision of 74.30 %. Mirnezami et al. (2021) combined deep learning and image-processing methods to extract tassel-flowering patterns from time-lapse camera images of plants grown under field conditions. Lu et al. (2021) used the TasselnetV3 model to count tassels in a public dataset and obtained rRMSE = 8.50 %. These studies showed that lightweight cameras and deep learning methods could be faster and more accurate in monitoring tassels.

Monitoring tassels raises several challenges, such as the small size of tassels on the image, the large number of tassels, and the complex background. When acquiring images of tassels, the weather conditions (e.g., cloud cover, temperature, moisture, and wind speed) affect the image quality, which makes it difficult to use RGB images to monitor tassels. However, the accuracy of crop monitoring may be improved by combining multiple features (Ji et al., 2020; Kumar et al., 2021). Compared with RGB images, multispectral Images are composites of images using more spectral bands. More spectral bands can provide spectrally informative insights, which would be very important for many applications, such as remote sensing, agriculture, environmental monitoring, etc (Zeng et al., 2020; Jin et al., 2022). The absorption and reflection properties of light were unique for different materials (Tucker, 1979). The common spectral information including spectral sensitive bands and vegetation indices. Red-edge band is used to identify and distinguish vegetation types (Tucker, 1979; Zeng et al., 2020), and vegetation indices with multi-band combinations are often used to represent the growth status of plants (environmental stress, disease determination, etc.) (Zeng et al., 2020; Cheng et al., 2021; Jin et al., 2022; Zeng et al., 2022; Tian et al., 2023). Therefore, Multispectral images have more spectral information than RGB images. Deep learning has powerful learning ability to effectively and automatically extract deep features, which has provided a new solution to extract hidden features from multispectral data. Hence, it is essential to investigate the application of deep learning segmentation methods to multispectral images of tassels, which should provide new insights on monitoring crop-growth status.

To summarize, developing a fast, large-scale, nondestructive method to quantify how tassels affect VIs is important for estimating the LAI. To fill gap in this knowledge, we use deep learning methods based on multispectral imagery to quantify how tassels affect LAI estimates. The objectives of this study are to (1) explore the feasibility of different coding structures of deep learning models for segmenting tassels on multispectral dataset; (2) quantify the contribution of tassels to VIs on multispectral dataset at the canopy scale; and (3) evaluate the difference between the original image and images removed tassels in estimating LAI and quantify the optimized number of VIs for estimating the LAI. This work provides a more accurate approach for monitoring the LAI of maize in field conditions, which has broad implications for improving crop management and ensuring food security.

2. Materials and methods

2.1. Site description

All experimentation was done at the Xinxiang Comprehensive Experimental Base, Xinxiang (113°47′E, 35°10′ N), Henan Province, China, which has a temperate continental climate with four distinct seasons. The annual average temperature is 14.1 °C and the average annual precipitation is 548.3 mm, mostly concentrated in July and August. Summer maize is one of the main crop varieties in the region. In this experiment, maize was sown on eight dates in 2020. [April 20 (No.1), April 30 (No.2), May 13 (No.3), May 23 (No.4), June 2 (No.5), June 14 (No.6), June 24 (No.7), and July 4 (No.8)]. Each plot was planted with three cultivars [Fengken 139 (FK139), Jingnongke 728 (JNK728), and Zhengdan 958 (ZD958)], and each cultivar covered 64 m^2 (22.5 m × 7.2 m) with a row spacing of 0.6 m and a planting density of 75 000 plants/hm^2. The study area location and planting diagram are shown in Fig. 1. Local field-management procedures were followed.

2.2. Data acquisition

In situ LAI data were acquired by using a SunScan canopy analysis system (Delta-T Devices Limited, U.K.), which consists of three components: a SunScan probe, a beam-fraction sensor, and a palmtop computer [Fig. 2(a)]. The parameters and measurement methods of SunScan have been detailed by Ogunbadewa et al. (2012). To eliminate experimental uncertainty, measurements were made from 10:00 to 14:00 on July 24, August 1, August 10, August 17, August 28, and September 2, 2020. The reported LAI was the average of four measurements made at the same positions of 0°, 45°, 90°, and 135°for each plot [Fig. 2(b)]. Representative plants of three cultivars were selected at random for measuring the LAI for the same sowing date, producing a total of 101 data.

The “fishing rod” phenotype remote-sensing platform [Fig. 3(a)] was equipped with a multispectral camera (RedEdge·MX) for image acquisition. The RedEdge·MX camera measured 8.7 cm × 5.9 cm × 4.54 cm and had a field of view of 47.2°. The multispectral images contained five bands: blue (475 ± 10 nm), green (560 ± 10 nm), red (668 ± 10 nm), Near Infrared (840 ± 20 nm), and red edge (717 ± 5 nm). For data acquisition, the multispectral camera was positioned 1.5 m above the top of the canopy, and two images were obtained: a normal-growth maize canopy [Fig. 3(d)], and the same image after manually removing the tassels [Fig. 3(e)]. The 202 images were pre-processed by cropping, alignment, and radiation calibration.

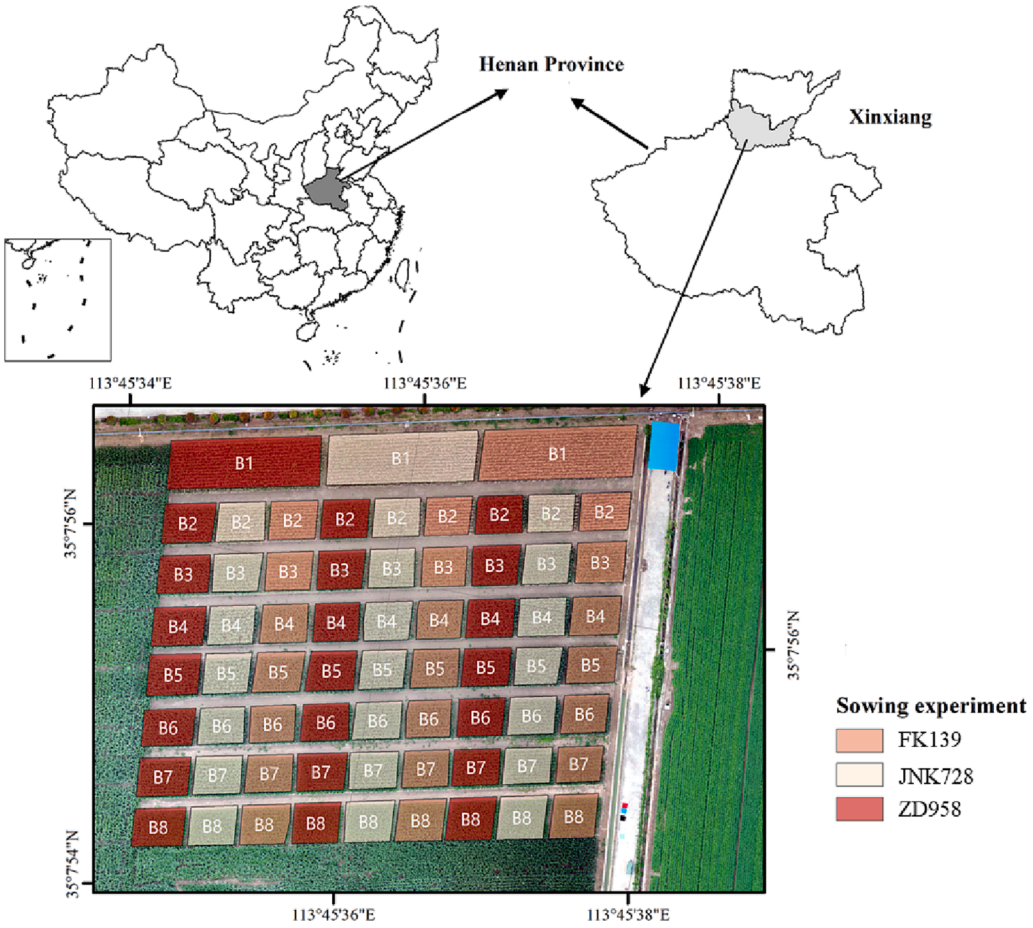

Fig. 1. Location and design of study area.

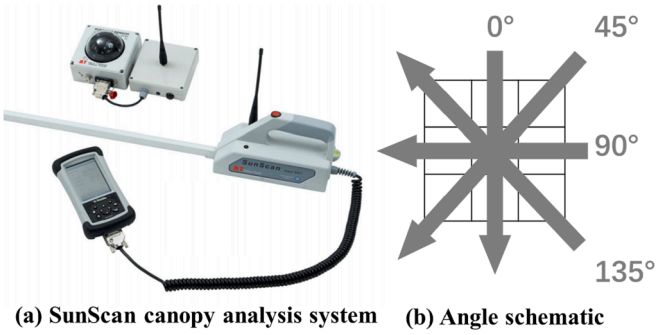

Fig. 2. The Acquisition Process of LAI.

2.3. Image-segmentation method

In this work, images are classified into three categories based on the tassel growth stage: early stage of tassel growth (T1), middle stage of tassel growth (T2), and late stage of tassel growth (T3). *Labelme* software was used to label the tassels, which were divided into two classes: tassels and background. To adequately explore the tassel features in multi-spectral imagery, multispectral dataset was established in this paper inspired by the study of Kumar et al. (2021). The multispectral dataset fused the blue, green, red, red edge, and near-infrared bands.

The U-Net model was proposed by Ronneberger et al. (2015) and consists of an encoder and decoder presenting a U-shaped structure. The U-Net model improves the segmentation accuracy by using a skip connection to fuse multiple features in the up-sampling process. U-Net models have been widely used for feature-extraction networks such as VGG16, MobileNetV2, ResNet50, InceptionV3, and Xception, etc. MobileNetV2 is a lightweight network proposed by Sandler et al. (2018), which is featured by the introduction of a reverse residual structure and a small number of parameters. ResNet solved the problem whereby excessive layers make the gradient disappear during training and make the network parameters drop rapidly (He et al., 2016). The present study compares the performance of the three coding structures VGG16, ResNet, and MobileNet for segmenting tassels. The image is cropped to 256 * 256 pixels to preserve image resolution. Based on the study of Garcia-Garcia et al. (2017), we selected the class pixel accuracy (CPA) and mean intersection over union (MIoU) as indicators of image-segmentation accuracy. The code was executed on a Windows 64-bit operating system, and training was done with a Keras 2.15 deep learning framework, which is an open-source framework from Google. We used an Intel Xeon(R) Gold 6132 CPU @ 2.60 GHz, a NVIDIA Quadro P5000 GPU, and 64 GB RAM.

2.4. Vegetation indices

Vegetation indices (VIs) are regarded as the feature combination of spectral information. The reflectance in multiple bands is mathematically transformed to enhance vegetation information and minimize non-vegetation signals (Bolton and Friedl, 2013; Metternicht, 2003; Marcial-Pablo et al., 2019). Table 1 lists the VIs calculated from multi-spectral imagery.

The results of image segmentation were divided into four categories: images of normal growing tassels (N), images acquired after removing tassels by hand (H), the estimation image after removing tassels (E), and images of tassels (T). The result of best U-Net model was used to mask

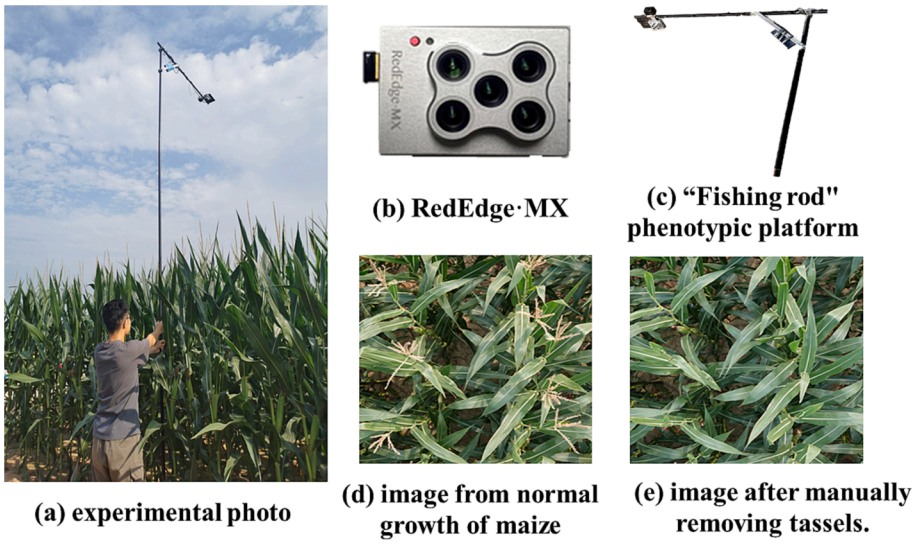

Fig. 3. Examples of image-acquisition procedure.

Table 1
Summary of vegetation indices calculated from multispectral images.

Vegetation index	Formula	Author
Triangular vegetation index (TVI)	$TVI = 60 \times (Band_{NIR} - Band_G) - 100 \times (Band_R - Band_G)$	Broge and Leblanc (2001)
Optimized soil-adjusted vegetation index (OSAVI)	$OSAVI = \frac{(Band_{NIR} - Band_R) \times 1.16}{Band_{NIR} + Band_R + 0.16}$	Rondeaux et al. (1996)
MERIS Terrestrial Chlorophyll Index (MTCI)	$MTCI = \frac{Band_{NIR} - Band_{Red\ -\ edge}}{Band_{Red\ -\ edge} - Band_R}$	Dash and Curran (2004)
Plant Pigment ratio (PPR)	$PPR = \frac{(Band_G - Band_B)}{(Band_G + Band_B)}$	Metternicht (2003)
Structure-insensitive pigment index (SIPI)	$SIPI = \frac{(Band_{NIR} - Band_B)}{(Band_{NIR} - Band_R)}$	Pen Uelas et al. (1995)
Red-edge chlorophyll index ($CI_{Red\text{-}edge}$)	$CI_{Red\ -\ edge} = \frac{Band_{NIR}}{Band_{Red\ -\ edge}} - 1$	Gitelson et al. (2005)
Red edge NDVI (NDVI_R)	$NDVI_{Red\ -\ edge} = \frac{Band_{NIR} - Band_{Red\ -\ edge}}{Band_{NIR} + Band_{Red\ -\ edge}}$	Gitelson and Merzlyak (1994)
Modified triangular vegetation index (MTVI2)	$MTVI2 = \frac{1.5 \times [1.2 \times (Band_{NIR} - Band_G) - 2.5 \times (Band_R - Band_G)]}{\sqrt{(2 \times Band_{NIR} + 1)^2 - (6 \times Band_{NIR} - 5 \times \sqrt{Band_R}) - 0.5}}$	Haboudane et al. (2004)
Green normalized difference vegetation index (GNDVI)	$GNDVI = \frac{Band_{NIR} - Band_G}{Band_{NIR} + Band_G}$	Gitelson and Merzlyak (1998)
Modified simple ratio (MSR)	$MSR = \frac{Band_{NIR}/Band_R - 1}{\sqrt{Band_{NIR}/Band_R} + 1}$	Xie et al. (2018)
Transformed chlorophyll absorption reflectance index (TCARI)	$TCARI = 3 \times \left[(Band_{Red\ -\ edge} - Band_R) - 0.2 \times (Band_{Red\ -\ edge} - Band_g) \times (\frac{Band_{Red\ -\ edge}}{Band_R})\right]$	Zarco-Tejada et al. (2002)
Enhanced vegetation index (EVI)	$EVI = 2.5 \times \frac{Band_{NIR} - Band_R}{Band_{NIR} + 6 \times Band_R - 7.5 \times Band_B + 1}$	Huete et al. (2002)
Modified chlorophyll absorption ratio index (MCARI)	$MCARI = (Band_{Red\ -\ edge} - Band_R - 0.2 \times (Band_{Red\ -\ edge} - Band_G)) \times (\frac{Band_{Red\ -\ edge}}{Band_R})$	Daughtry et al. (2000)
Soil-adjusted vegetation index (SAVI)	$SAVI = \frac{Band_{NIR} - Band_R}{Band_{NIR} + Band_R + 0.5} \times 1.5$	Huete (1988)
Modified Soil-adjusted vegetation index (MSAVI)	$MSAVI = \frac{1.5 \times (Band_{NIR} - Band_{Red})}{(Band_{NIR} + Band_{Red} + 0.5)}$	Qi et al. (1994)
Modified non-linear vegetation index (MNLI)	$MNVI = \frac{1.5 \times (Band_{NIR}^2 - Band_R)}{Band_{NIR}^2 + Band_R + 0.5}$	Gong et al. (2003)
Difference vegetation index (DVI)	$DVI = BAND_{NIR} - BAND_R$	Jordan (1969)
Normalized difference vegetation index (NDVI)	$NDVI = \frac{Band_{NIR} - Band_R}{Band_{NIR} + Band_R}$	Rouse et al. (1973)
Ratio vegetation index (RVI1)	$RVI2 = \frac{Band_{NIR}}{Band_R}$	Daughtry et al. (2000)
Ratio vegetation index (RVI2)	$RVI2 = \frac{Band_{NIR}}{Band_G}$	Xue et al. (2004)

Note: $Band_R$, $Band_G$, $Band_B$, $Band_{NIR}$, $Band_{Red\text{-}edge}$ respectively denote the red band, green band, blue band, near-red band, and red-edge band.

the N images, and then obtain the E and T images (Fig. 4). VIs extracted from four image categories were used to explain how tassels affect canopy spectral information.

2.5. Quantifying the contribution of tassels

The contribution was quantified in the multispectral data based on the area of the tassels according to study by Shao et al. (2022). Due to the different image sizes obtained after clipping, standardization and normalization were needed to calculate the spectral contribution of tassels, which was calculated as follows:

$$CT = \frac{V_T \times S_T}{V_T \times S_T + V_L \times S_L}, \quad (1)$$

where V_T is the VI calculated based on the T images, S_T is the fraction of area in the images with tassels, V_L is the VI calculated from the leaves in the images, and S_L is the fraction area in the images with leaves. The contribution of the tassels to the canopy is mainly classified as positive and negative. For example, the vegetation index calculated from the tassel image is less than 0, the vegetation index calculated from the canopy images is greater than 0. In this case, the contribution of the tassels to the canopy is less than 0, the contribution of the tassels to the canopy is negative.

2.6. Method of estimate LAI

Five machine learning methods were selected to estimate the LAI [see details in Xu et al. (2021a), Liu et al. (2021) and Yang et al. (2021)]. These methods are implemented in the Python SKlearn package. We used partial least squares regression (PLSR), which is a regression method for treating multiple variables dependent on multiple independent variables (Kamboj et al., 2021). We also used support vector regression (SVR) to improve the generalizability of the proposed model by mapping the data to a high-dimensional feature space through a nonlinear mapping and finding the optimal hyperplane (Xu et al., 2021a). The radial basis kernel function was set as the SVR kernel function, and the penalty factor C was set to 1. We used the random forest (RF) algorithm based on a decision tree as the base classifier, with the mean value of each decision tree serving as the final result (Xu et al., 2021a). In this study, the decision tree was set to 100. We used a gradient-boosting decision tree (GBDT), which boosts iterations, and the residuals of the previous round of base learners were fit by the negative gradient of the loss function to gradually decrease the residual estimates of each round and thereby accelerate the convergence to the local or global optimal solution (Yang et al., 2021). The GBDT was set to 100 decision trees with the mean squared error serving as loss function, and the learning rate was set to 0.1.

A deep neural network (DNN) is a multilayer perceptron containing several hidden layers with excellent nonlinear processing capability and can abstract valuable high-level feature information from low-level features (Jin et al., 2020b; Liu et al., 2021; Xu et al., 2021a). Given its efficient processing capability, the DNN network was used as regression model. Fig. 5 shows the structure of the DNN network.

The DNN network structure consists of an input layer, a hidden layer, and an output layer. There are 20 neurons in the input layer and one neuron in the output layer. There are six layers in the hidden layer, and the neurons in each layer number on the order of 128, 64, 32, 16, 8, and 4. The activation function is

$$\tanh(x) = \frac{e^x - e^{-x}}{e^x + e^{-x}}, \quad (2)$$

and the mean squared error serves as the loss function. In Eq. (2), tanh applies to the case of output symmetry and takes values in the range [−1, 1], with zero being the mean value.

Twenty VIs were selected for estimating the LAI using different machine learning methods. 80 % of the dataset (80 samples) was selected for model building, and 20 % of the dataset (21 samples) was used for model validation. The coefficient of determination, R^2, RMSE, and rRMSE were selected to evaluate the training and validation models. R^2, the RMSE, and the rRMSE were as calculated as follows:

$$R^2 = \frac{\sum_{i=1}^{n}(x_i - \overline{x})^2 \times (y_i - \overline{y})^2}{\sum_{i=1}^{n}(x_i - \overline{x})^2 \times \sum_{i=1}^{n}(y_i - \overline{y})^2}, \quad (3)$$

$$RMSE = \sqrt{\frac{\sum_{i=1}^{n}(y_i - x_i)^2}{n}}, \quad (4)$$

$$rRMSE = \frac{RMSE}{\overline{x}}, \quad (5)$$

where x_i and y_i are the measured and predicted values, respectively, $\overline{x}$ and $\overline{y}$ are the mean measured and predicted values, respectively, and n is the number of samples.

3. Results

3.1. Tassel segmentation

To assess the accuracy of tassel segmentation from multispectral dataset, Table 2 showed the performance of the three encoding structures of the U-Net model (Resnet, MobileNet and VGG). The U-Net coding structure accuracy (MIoU and CPA) in descending order was VGG, Resnet, and MobileNet. The highest accuracy was thus VGG (CPA varies from 86.82 to 89.01, and MIoU varies from 75.5 to 89.01). Ranking in descending order according to MIoU segmentation accuracy given T2, T1, T3. The area of the tassels was larger in the middle of tassels growth, and the features of the tassels were more obvious (Fig. 6). In the late stages tassel growth leaves gradually turned yellow, which was similar to the tassels color. Hence, the U-Net model had some limitations in identifying tassels, resulting in the formation of noise on the pictures in the late stages tassel growth (Fig. 6). The VGG-encoded U-Net model was more robust for tassel segmentation during T2 (MIoU = 89.53 %, PA = 85.97 %, Fig. 6).

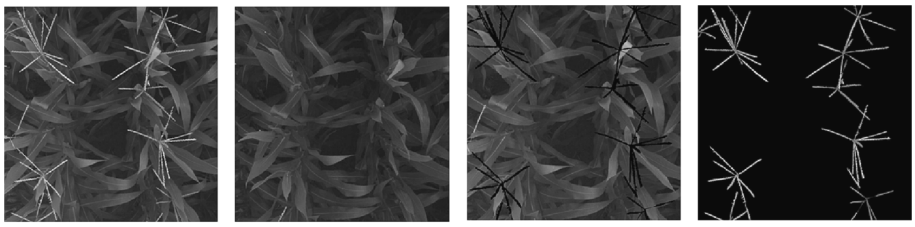

Fig. 4. Four categories of tassel images.

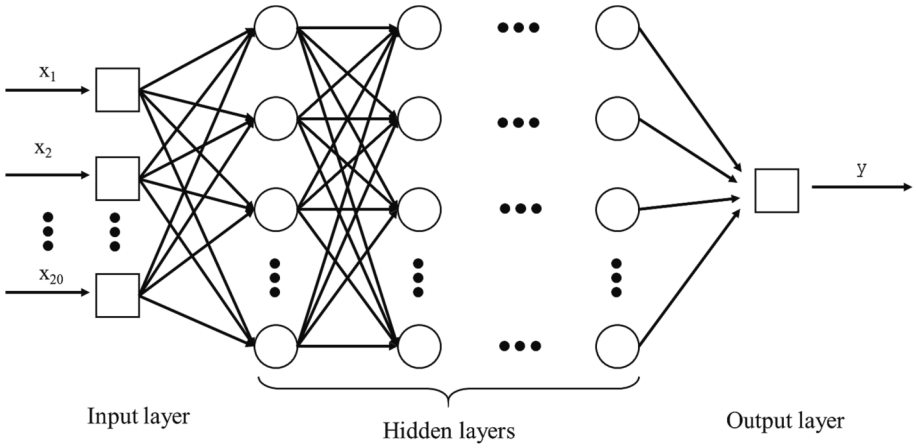

Fig. 5. DNN network structure.

Table 2
Accuracy of prediction by UNet.

Time	Metric (%)	Encoder structure		
		Resnet	MobileNet	VGG
T1	CPA	89.31	88.95	**89.01**
	MIoU	79.92	78.47	**81.94**
T2	CPA	89.07	86.96	**89.53**
	MIoU	85.47	82.94	**85.97**
T3	CPA	82.37	76.47	**86.82**
	MIoU	**76.63**	73.6	75.5

Note: T1, T2, and T3 represent early stage tassel growth, middle stage tassel growth, and late stage tassel growth.

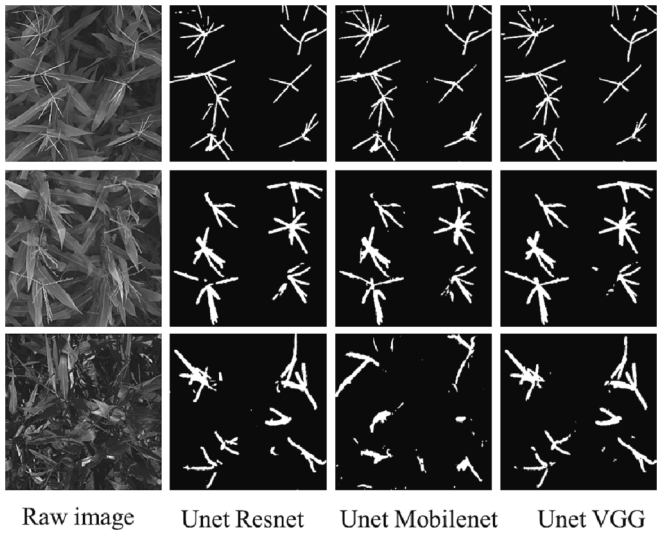

Fig. 6. Estimation results of the VGG coding structure of U-Net. Note: Images arranged top to bottom correspond to early tassel growth, mid tassel growth, and late tassel growth, respectively.

3.2. Contribution of tassels

The four image categories (N, H, E, and T) were used to investigate how tassels affect VIs for three maize cultivars and over three growth stages (Fig. 7). The VIs tends to decrease with the maize growth. Ranking in descending order of cultivars according to VI gives ZD958, JNK728, and FK139. The VIs of T images were lower than those obtained from N and E images. The difference in VIs calculated from N and T images ranged from 1.83 % to 127.31 %, and the difference was largest for the MNLI, which indicated that tassels can influence the canopy spectral information. The difference in VIs between image E and image H varied from 0.11 % to 43.32 %, which indicated that the proposed algorithm significantly mitigated the effect of tassels on VIs.

Tassels of different cultivars have different structural and spectral information at different growth stages, which impacts the canopy spectral information. Therefore, the contribution of tassels to different VIs was quantified according to Eq. (1), and the results were shown in Fig. 8. The contribution of VIs (except for TVI, OSAVI, DVI, PPR, TCARI, MNLI, and MCARI) for FK139 was increased and then decreased with maize growth and was higher at the end of tassel growth than at the beginning of tassel growth. The contribution of VIs (SIPI, NDVI, MSR, OSAVI, DVI, EVI, MNLI, SAVI, and MSAVI) was decreased first and then increased. Ranking in descending order according to the contribution of the different cultivars given JNK728, ZD958, and FK139. Tassels make their largest contribution to the SIPI for JNK728 during the middle tassel-growth stage (9.73), and their smallest contribution was to the MNLI for ZD958 during the end of tassel growth (−2.99).

3.3. Effect of tassels on LAI estimation

The accuracy of LAI estimates was determined by the input variables and regression models. Vegetation index, as a commonly used input variable, is sensitive to environment in the estimation process. Therefore, it was necessary to study the effects of different environmental datasets on the accuracy of LAI estimation. To investigate how tassels affect estimates of the LAI, VIs calculated from the three image categories (N, H, and E) were used to estimate the LAI using machine learning methods (see Section 2.6). In general, the best performance in estimating LAI was when using the GBDT, followed by RFR, SVR and PLSR. The accuracy of LAI estimates differed for different datasets. Ranking the datasets in descending order according to R^2 given E images, N images, and H images. The measured LAI ranged from 0.8 to 6.5. PLSR, SVR and RFR have underestimated LAI, and the estimated range of LAI was smaller than the measured LAI (Fig. 9). The most accurate LAI estimate was estimated by the GBDT method on the E dataset (R^2 = 0.816, RMSE = 39.9 % and rRMSE = 7.4 %). The accuracy of the estimated LAI be significantly improved by removing tassels.

The trait of deep learning is automatic feature extraction. Using the DNN method to estimate the LAI from the three datasets and then ranking the results in descending order in terms of R^2 given the E dataset, N dataset, and H dataset (Fig. 10). The VIs extracted from the E dataset had the highest accuracy in estimating LAI (R^2 = 0.799, RMSE = 41.6 %, rRMSE = 11.2 %). Using DNN model have lower accuracy in estimating LAI than the above machine learning methods because deep learning requires a larger data than used in this work. In future studies,

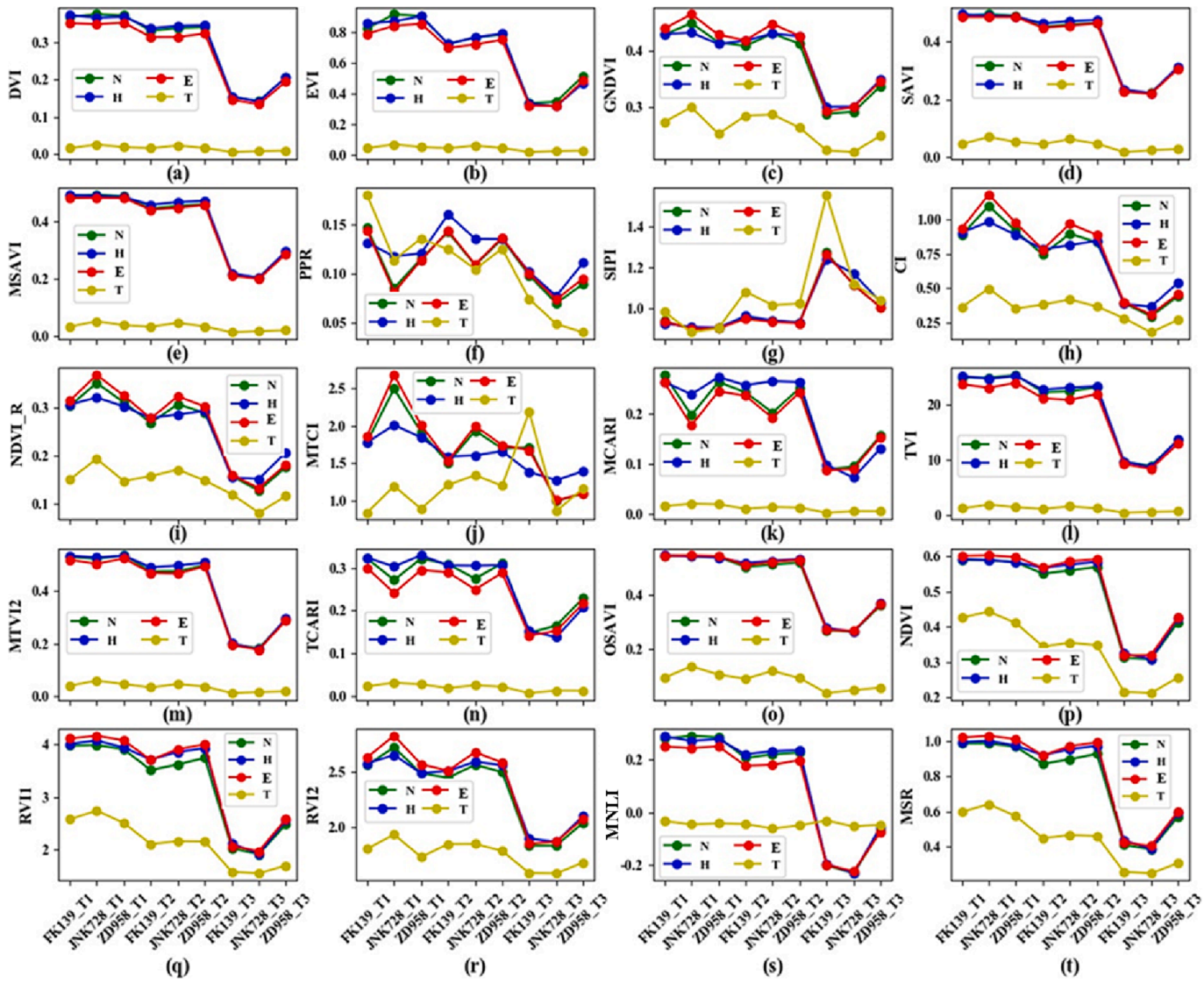

Fig. 7. Vegetation indices for four types of images and for three cultivars during the three growth stages. Note: T1, T2, and T3 denote the early, middle, and end stage of tassel growth, respectively. Labels N, H, E, and T represents images of normal growing tassels, images acquired after removing tassels by hand, the estimation image after removing tassels, and images of tassels, respectively.

the use of the DNN method to estimate the LAI will be further evaluated with more data.

The selection of vegetation indices is complicated and time-consuming, and it is limited for single vegetation index to represent vegetation information. More vegetation indexes can make full use of vegetation information, but it results in some information redundancy. Hence, it is critically importance to select the amount of the appropriate vegetation indices. To determine how the number of VIs affects the accuracy of LAI estimates, we ranked them in descending order of the tassel contribution: MNLI, DVI, TVI, MCARI, EVI, TCARI, MSAVI, MTVI2, SAVI, OSAVI, CI, MSR, NDVI_R, RVI1, NDVI, GNDVI, MTCI, RVI2, PPR, and SIPI. The VIs extracted from the dataset were sequentially put into the GBDT model to estimate the LAI. Fig. 11 showed that the training datasets produced better results than the testing dataset. The accurately of LAI estimation became stable when using the following nine VIs as variables: MNLI, DVI, TVI, MCARI, EVI, TCARI, MSAVI, MTVI2, SAVI, at which the test R^2, RMSE and rRMSE of estimated LAI were 0.824, 40.7 % and 10.9 %, respectively.

4. Discussion

To improve the accuracy of segmenting tassels in the field, this study introduced multispectral datasets. For tassels segmentation, the current methods have been based on RGB data, such as HSeg (Tang et al., 2011), mTASSEL-S (Lu et al., 2015) and the region-based color model (Lu et al., 2016) and the recently introduced U-Net model (Shao et al., 2022). But the background of tassels is more complex in the field environment, which increases the difficulty of the tassels segmentation. Compared with RGB images, Multispectral images have more spectral bands, the band customization of multispectral sensors requires higher efforts and the images have been processed by complex image processing, such as correction and alignment processes. Nevertheless, multispectral images could provide more spectral information, and the information could reflect the growth status of vegetation. Deep learning can automatically extract its features, which provided the opportunity to using multispectral images. Hence, we compared the performance of different coding structures of the U-Net model using multispectral images. The proposed VGG-encoded U-Net model based on multispectral data achieved better accuracy in tassels segmentation (CPA = 89.53 %, MIoU = 85.97 %), which was better than the accuracy of tassels segmentation

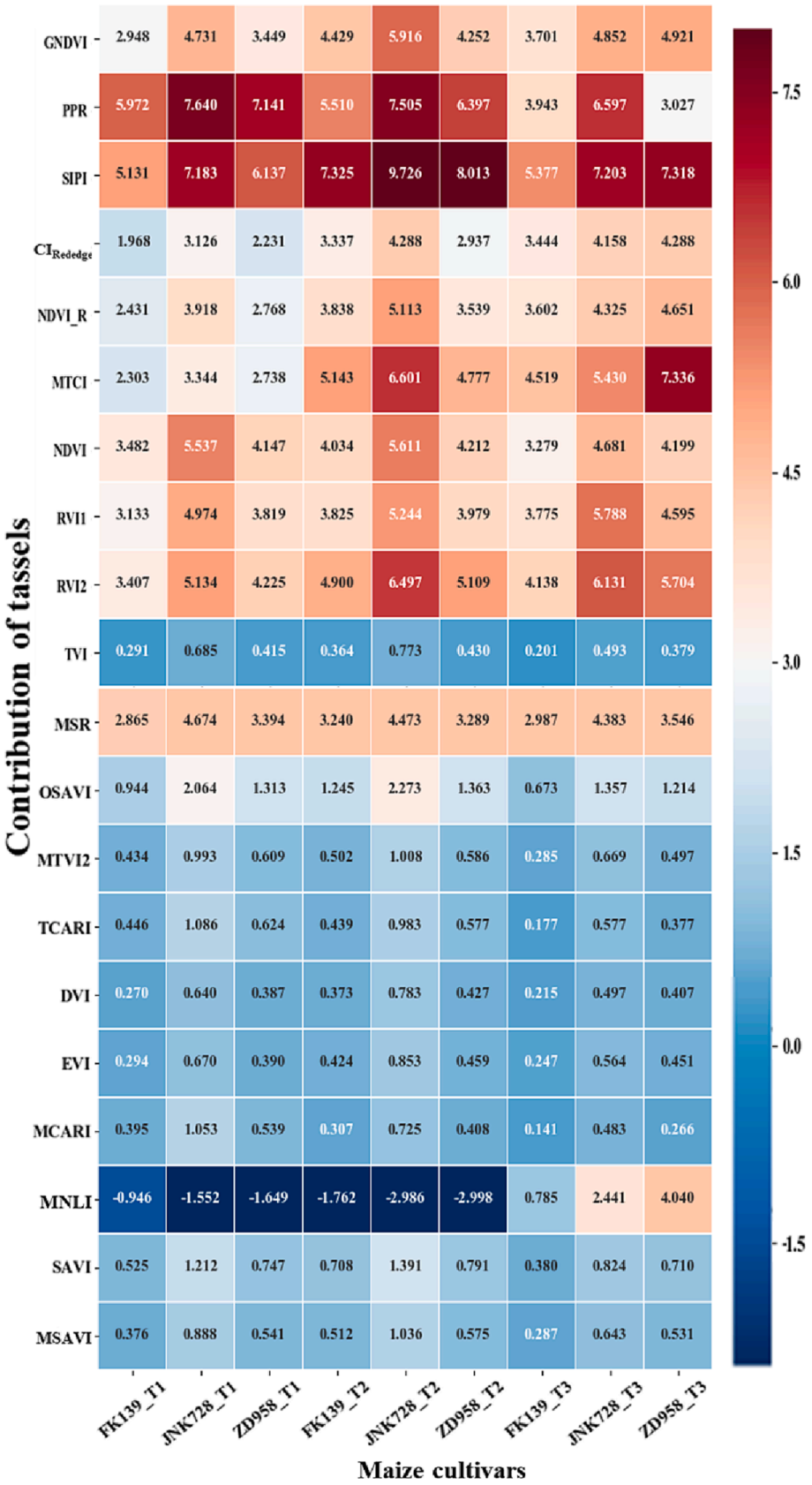

Fig. 8. Contribution of tassels to VIs from multispectral imagery. Note: T1, T2, and T3 represent the early, middle, and end of tassel growth, respectively.

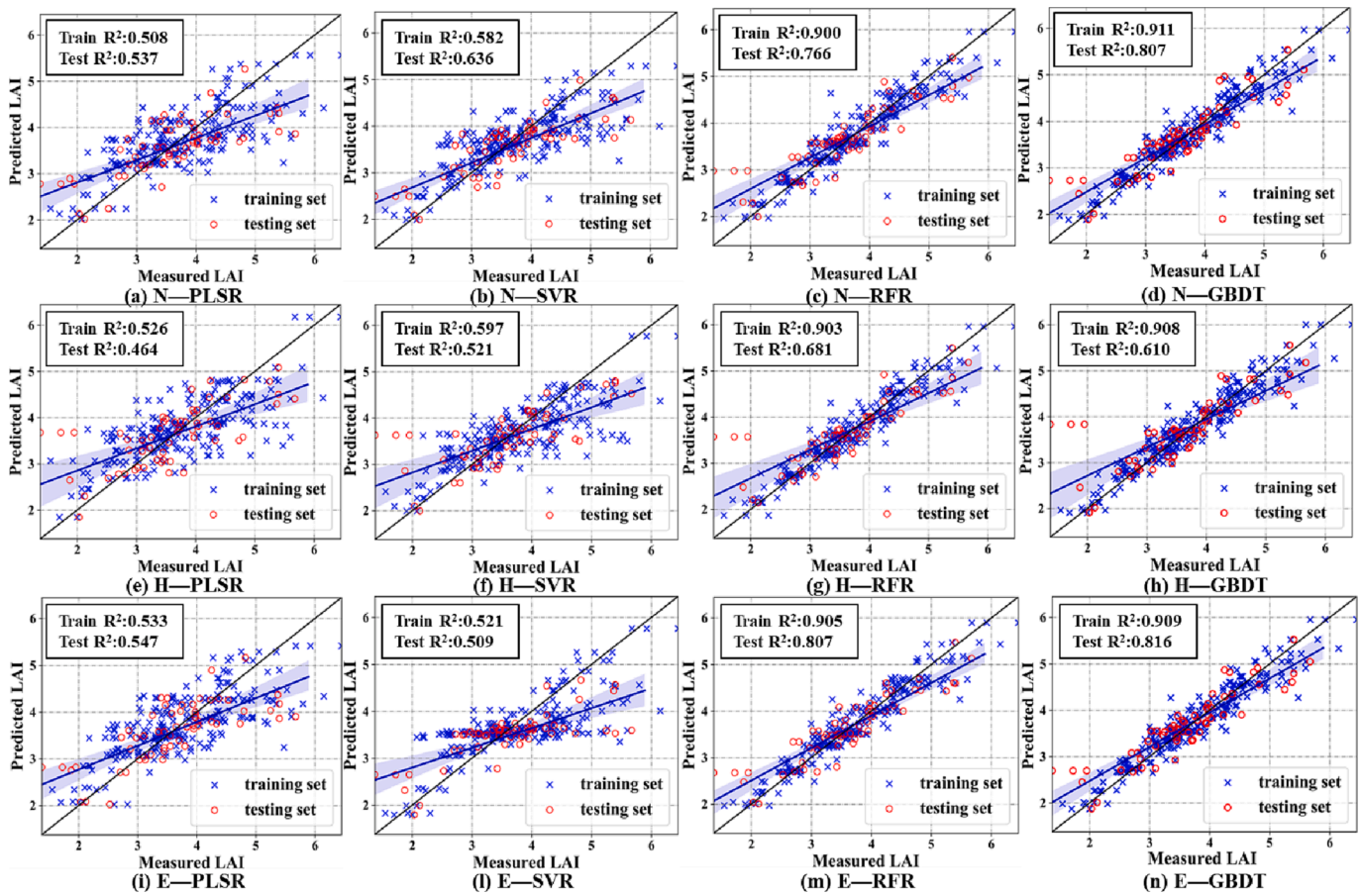

Fig. 9. Results of estimated LAI. Note: Labels N, H, and E refer to images of normal growing tassels, images with tassels removed by hand, and the estimation image after removing tassels.

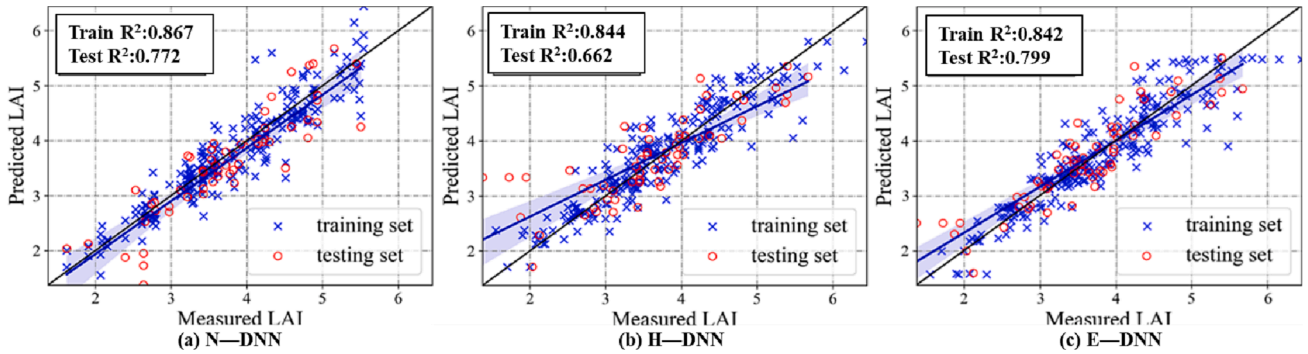

Fig. 10. LAI estimated by deep learning model. Note: Labels N, H, and E refer to images of normal growing tassels, images with tassels removed by hand, and the estimation image after removing tassels.

based on RGB data (CPA = 82.14 %, MIoU = 84.43 %) (Shao et al., 2022). Multispectral images can not only identify differences in morphology and structure of features, but can also increases tassels feature based on differences in spectral characteristics (Kumar et al., 2021). The VGG16 is the most accurate coding structure in the U-Net model, mainly because VGG16 encoding has numerous parameters (24 M) to detect more complex features. In the present work, the multi-spectral dataset improves the accuracy of tassel segmentation, which is consistent with the findings of Kumar et al. (2021). With the growth of maize, the accuracy of the U-Net model for segmenting tassels first was increased and then decreased. The reason is that the water content and chlorophyll of the tassels are most different from the leaves during the T2 period, which contributes to the distinctly different spectrum of the tassels from the leaves. In future studies we will further explore the reasons for this phenomenon by measuring the differences in water content and chlorophyll of tassels and leaves during various growth periods.

To quantify more accurately the contribution of tassels to the canopy spectral information, Fig. 12 showed the change in reflectance of the image. Tassels contributed more to VIs for the JNK728 cultivar than for the ZD958 or FK139 cultivar (Fig. 8). The contribution of the tassels varied among maize cultivars, which was mainly attributed to differences of area (morphological differences: height, size, aggregation, tassels length, etc.) and spectral differences of the tassels (Eq.1). The change in reflectance of the four types of images was obtained for further study of the spectral changes after removal of the tassels

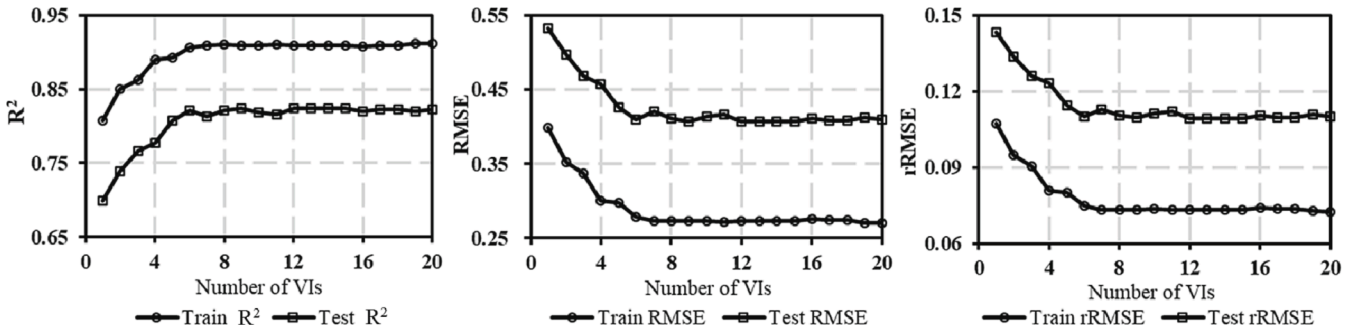

Fig. 11. Accuracy of estimation of GBDT model as a function of number of VIs.

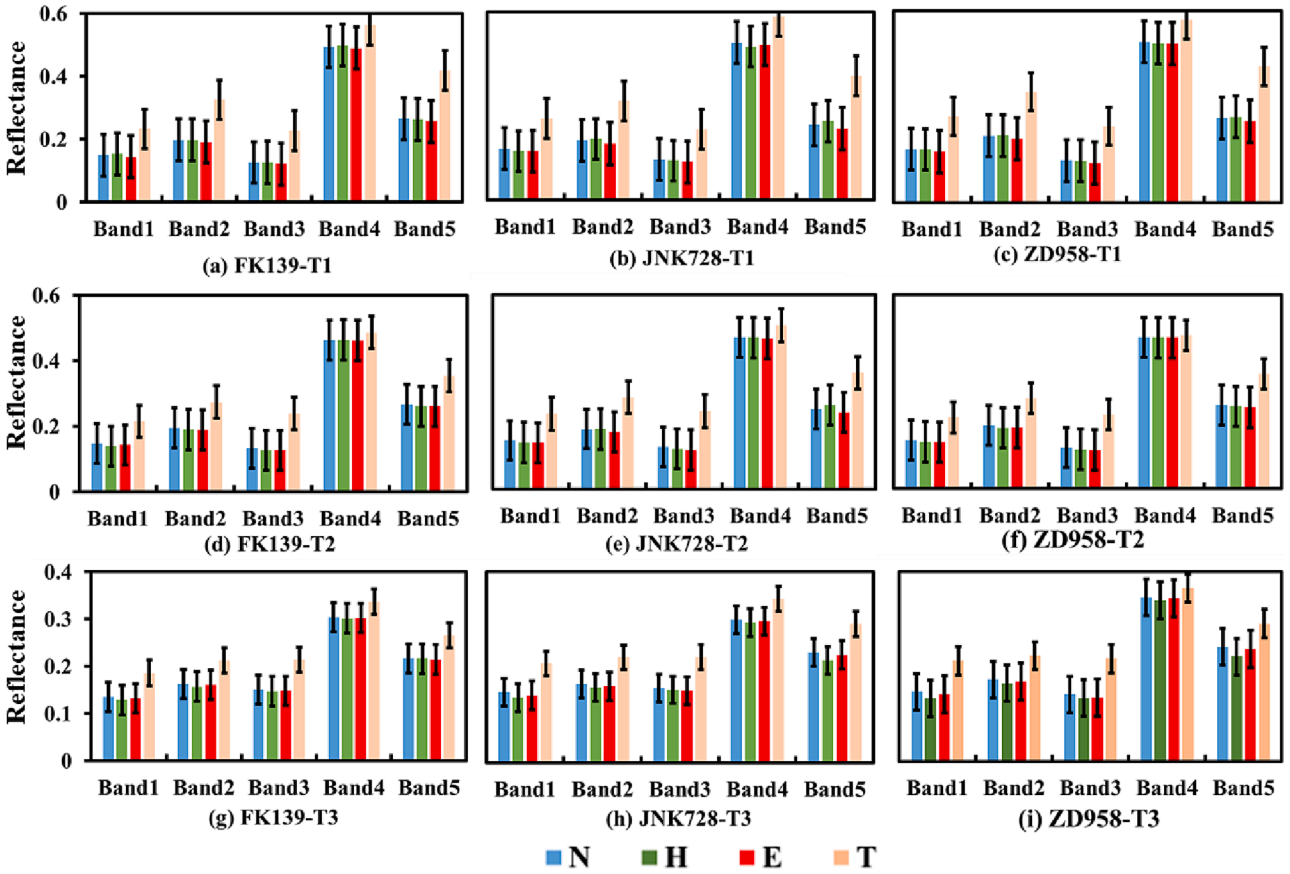

Fig. 12. Reflectance of cultivars for different types of images. Note: Labels N, H, E, and T indicate images of normal growth tassels, images with tassels removed by hand, the estimation image after removing tassels, and images with tassels, respectively.

(Fig. 12). The datasets in descending order of spectral reflectance were T, N, E, and H. The tassels enhanced the reflectance of each band, so the reflectance was decreased significantly upon removing the tassels. The E image was obtained by masking the results of the U-Net model segmentation, whereby the vegetation index calculated from the E image excludes the tassels component (Fig. 4). The reflectance (T Images) of the tassels was different in each band (Fig. 12), therefore the vegetation index calculated from the E images after the removal of the tassels and N images of normal growing tassels also differed a certain extent. The differences in vegetation index based on the E images were affected by two factors: the area of the tassels and the formulas of the vegetation index. At the early stages the area of tassels was small, it showed a yellowish color and tassels influences the reflectance to a minor extent, as the area of the tassels grew larger the tassels influenced the reflectance to a greater extent. The tassels mainly influenced the red-edge band (Fig. 12), which resulted in greater variation in NDVI_R, MTCI, CI, TCARI, MTCI, MCARI with stage of tassels growth (Fig. 7). Therefore, the reflectance of the E image was significantly lower relative to that of the N image, which indicated that the segmentation algorithm removes the tassels from the image can reduce the effect of tassels on the canopy reflectance. However, the present method has some limitations in the early stage of the tassels. At the early stages of tassels, the area of the tassels was small and the contribution of the tassels to the canopy reflectance was little (Figs. 8 and 13). Therefore, the difference between the vegetation indices calculated on the basis of image E and image N was small at the early stages of tassels growth, the results of the estimated LAI ware not significantly different. The studies of Jin et al. (2020b) and Bai et al. (2019) has shown that the difference in water content and chlorophyll content of the tassels was leading to the fact that the reflectance of the tassels was significantly different from that of leaves. The apparent differences in VIs between H images and E images are due to (1) the loss of leaves upon manually removing tassels, (2) the

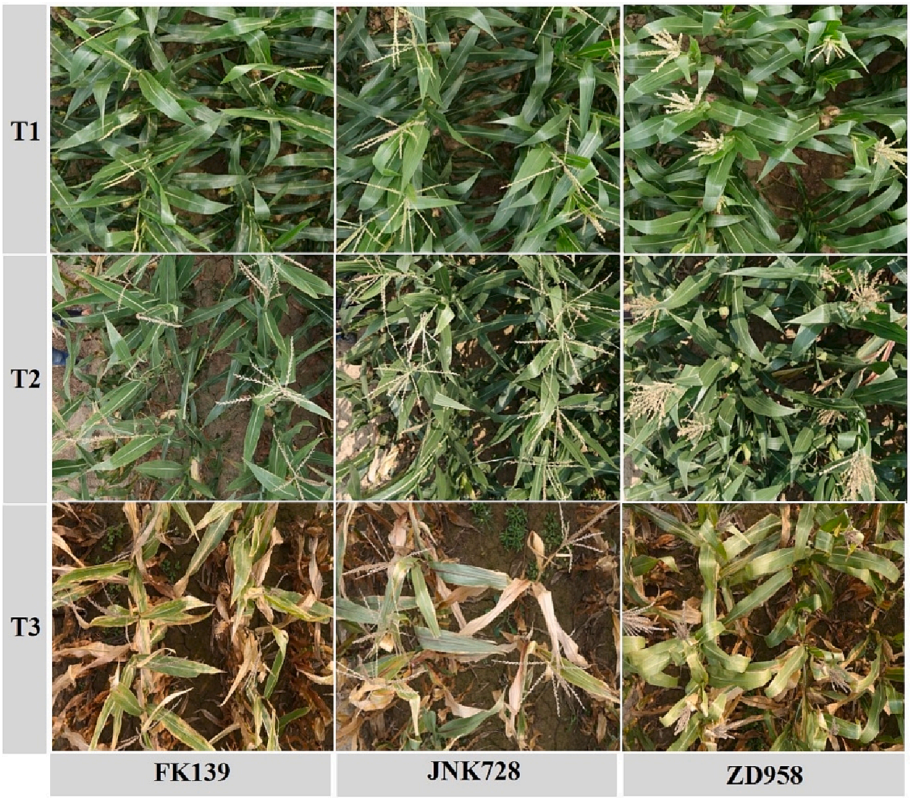

Fig. 13. The image of tassels. Note: T1, T2, and T3 represent the early, middle, and end of tassel growth, respectively.

change in maize canopy structure due to manual error, and (3) the changes in chlorophyll content and nitrogen content of maize leaves after removal of tassels. Therefore, in future studies, we will quantify how the chlorophyll, water content, and nitrogen of leaves and the canopy structure vary upon removing the tassels.

The LAI was estimated by combining machine learning methods and VIs extracted from N, H, and E images. The GBDT method for the E dataset ($R^2 = 0.816$, RMSE = 39.9 % and rRMSE = 7.4 %) was able to the most accurately estimate LAI. The GBDT model was based on the boosting algorithm, which can minimize the loss in the prediction process (Yang et al., 2021). Hence, the GBDT model has better robustness in estimating LAI. The study of Jin et al. (2020a) has shown that DNN methods required a large amount of training data to estimate crop parameters indicating that we need more data to optimize the DNN model in follow-up research. Hence, for estimating the LAI, the DNN method was slightly less accurate than the GBDT method. Yang et al. (2021) used the GBDT method to accurately estimate the leaf nitrogen content, and current studies estimated crop parameters by calculating VIs with tassels and leaves treated as single integrated objects. However, Bai et al. (2019) showed that tassels significantly affect the canopy reflectance in the green and red bands, which is consistent with the present results. Therefore, the purpose of estimating the LAI using three datasets (N, H and E) is to investigate how tassels affect the estimation of the LAI. The R^2 of image E was significantly improved by 1.2 % and rRMSE was decreased by 1.3 % compared with image N (Fig. 9), which indicated that removing the tassels using the proposed image algorithm could improve the accuracy of LAI estimates.

A single parameter can only represent limited information about crop growth (Xu et al., 2021a), hence the combination of multiple variables should improve the accuracy of estimates of crop parameters. For example, Liu et al. (2021) showed that the use of multiple VIs and structural indices (e.g., canopy cover, texture information, canopy thermal information) enhanced the accuracy of LAI estimates. Xu et al. (2021b) used an improved fuzzy comprehensive evaluation method to construct a comprehensive yield evaluation indicator from hyperspectral data and agronomic parameters, which improves the accuracy of yield estimates. However, the challenge in multivariate estimates of crop parameters is that information redundancy between VIs often affects calculation time and accuracy. Thus, using an appropriate number of VIs is essential. This study identified the nine VIs for estimating LAI by contribution of tassels to the canopy. The types of vegetation indices include the ratio vegetation index, the difference vegetation index, etc. The accuracy of estimating LAI was varied with the type of vegetation index was determined without distinguishing the type of vegetation index, which would have some limitations (Tan et al., 2013; Morel et al., 2014; Putzenlechner et al., 2019). For maize, the tassels made up a larger percentage of the canopy (Fig. 4). Therefore, this work presented a new perspective that determined the number of selected vegetation indices for estimating LAI based on the tassel contribution. It is essential to combine more crop parameters (agronomic parameters, VI, and textures) from different regions and the order of different variables to improve the robustness of this method, which can provide a technical support for crop growth status monitoring in future studies.

5. Conclusion

Accurately estimating LAI is important for monitoring maize growth status. Tassels spectral information is clearly different from canopy, which leads to bias in LAI estimation using canopy spectra. In this study, Image-segmentation methods and regression methods (PLSR, SVR, RFR, GBDT, DNN) were combined to quantify how tassels affect the VIs and the accuracy of estimates of the LAI. The main conclusions are as follows:

(1) The VGG-encoded U-Net model provided the most accurate method to segment tassels on the multispectral dataset (CPA = 89.53 %, MIoU = 85.97 %). The accuracy of the segmented tassels was first increased and then decreased with tassel growth.

(2) Applying the image algorithm for removing tassels significantly alleviated the negative effect of tassels on the canopy spectrum. In descending order, the VIs contributed to by tassels are MNLI, DVI, TVI, MCARI, EVI, TCARI, MSAVI, MTVI2, SAVI, OSAVI, CI, MSR, NDVI_R, RVI1, NDVI, GNDVI, MTCI, RVI2, PPR, and SIPI. The contribution of tassels to VIs for the JNK728 cultivar was greater than that of the ZD958 or FK139 cultivar.

(3) The most accurate LAI estimates were obtained from the E dataset with tassels removed by the image algorithm when using the GBDT method ($R^2 = 0.816$, RMSE = 39.9 % and rRMSE = 7.4 %). The accuracy of LAI estimates was most stable when using the nine VIs selected in order of tassel contributions to VIs. The results of this study showed the significant potential of multispectral image segmentation of tassels. Removing tassels and quantifying the number of VIs can significantly improve the accuracy of LAI estimation. These results provided new perspectives and technical references for monitoring crop growth for both farmers and researchers.

Credit authorship contribution statement

Mingchao Shao: Conceptualization, Methodology, Software, Writing - review & editing. **Chenwei Nie**: Conceptualization, Methodology, Software, Writing - review & editing. **Aijun Zhang**: Project administration - review & editing. **Liangsheng Shi**: Data curation. **Yuanyuan Zha**: Data curation. **Honggen Xu**: Data curation. **Hongye Yang**: Data curation. **Xun Yu**: Data curation. **Yi Bai**: Data curation. **Shuaibing Liu**: Data curation. **Minghan Cheng**: Data curation. **Tao Lin**: Investigation. **Ningbo Cui**: Investigation. **Wenbin Wu and Xiuliang Jin**: Project administration and Funding acquisition.

Declaration of Competing Interest

The authors declare that they have no known competing financial interests or personal relationships that could have appeared to influence the work reported in this paper.

Data availability

Data will be made available on request.

Acknowledgments

This research was supported by Central Public-interest Scientific Institution Basal Research Fund for Chinese Academy of Agricultural Sciences (CAAS-ZDRW202107), Key Cultivation Program of Xinjiang Academy of Agricultural Sciences (xjkcpy-2020003), National Natural Science Foundation of China (42071426, 51922072, 51779161, 51009101), the Agricultural Science and Technology Innovation Program of the Chinese Academy of Agricultural Sciences, Nanfan special project, CAAS (ZDXM2310, YBXM01), Hainan Yazhou Bay Seed Lab (GBGS + B21HJ0221), and The State Key Laboratory of Water Resources and Hydropower Engineering Science (2021NSG01).

References

Andrimont, D.R., Taymans, M., Lemoine, G., Ceglar, A., Yordanov, M., van der Velde, M., 2020. Detecting flowering phenology in oil seed rape parcels with Sentinel-1 and -2 time series. Remote Sens. Environ. 239, 111660.

Bai, L., Bai, J., Xiao, Q., 2019. Effects of maize tassel at the heading stage on radiation transfer characteristics of canopy reflectance. Trans. Chin. Soc. Agric. Eng. https://doi.org/10.11975/j.issn.1002-6819.2019.20.020.

Bolton, D.K., Friedl, M.A., 2013. Forecasting crop yield using remotely sensed vegetation indices and crop phenology metrics. Agric. For. Meteorol. 173, 74–84.

Breda, N.J., 2003. Ground-based measurements of leaf area index: a review of methods, instruments and current controversies. J. Exp. Bot. 54, 2403–2417.

Broge, N.H., Leblanc, E., 2001. Comparing prediction power and stability of broadband and hyperspectral vegetation indices for estimation of green leaf area index and canopy chlorophyll density. Remote Sens. Environ. 76 (2), 156–172.

Cao, Z., Cheng, T., Ma, X., Tian, Y., Zhu, Y., Yao, X., Chen, Q.i., Liu, S., Guo, Z., Zhen, Q., Li, X., 2017. A new three-band spectral index for mitigating the saturation in the estimation of leaf area index in wheat. Int. J. Remote Sens. 38 (13), 3865–3885.

Cheng, M., Jiao, X., Li, B., Yu, X., Shao, M., Jin, X., 2021. Long time series of daily evapotranspiration in China based on the SEBAL model and multisource images and validation. Earth Syst. Sci. Data 13, 3995–4017.

Dash, J., Curran, P.J., 2004. The MERIS terrestrial chlorophyll index. Int. J. Remote Sens. 25 (23), 5403–5413.

Daughtry, C.S., Walthall, C.L., Kim, M.S., De Colstoun, E.B., McMurtrey Iii, J.E., 2000. Estimating corn leaf chlorophyll concentration from leaf and canopy reflectance. Remote Sens. Environ. 74, 229–239.

Dimitrov, P., Kamenova, I., Roumenina, E., Filchev, L., Ilieva, I., Jelev, G., Gikov, A., Banov, M., Krasteva, V., Kolchakov, V., Kercheva, M., Dimitrov, E., Miteva, N., 2019. Estimation of biophysical and biochemical variables of winter wheat through Sentinel-2 vegetation indices. Bulgarian J. Agr. Sci. 25, 819–832.

Garcia-Garcia, A., Orts-Escolano, S., Oprea, S., Villena-Martinez, V., Garcia-Rodriguez, J., 2017. A review on deep learning techniques applied to semantic segmentation. *arXiv preprint arXiv:1704.06857*.

Gitelson, A., Merzlyak, M.N., 1994. Spectral reflectance changes associated with autumn senescence of *Aesculus hippocastanum* L. and *Acer platanoides* L. leaves. Spectral features and relation to chlorophyll estimation. J. Plant Physiol. 143, 286–292.

Gitelson, A.A., Merzlyak, M.N., 1998. Remote sensing of chlorophyll concentration in higher plant leaves. Adv. Space Res. 22 (5), 689–692.

Gitelson, A.A., Vina, A.E.S., Ciganda, V.O.N., Rundquist, D.C., Arkebauer, T.J., 2005. Remote estimation of canopy chlorophyll content in crops. Geophys. Res. Lett. 32, L08403.

Gong, P., Pu, R., Biging, G.S., Larrieu, M.R., 2003. Estimation of forest leaf area index using vegetation indices derived from Hyperion hyperspectral data. IEEE Trans. Geosci. Remote Sens. 41, 1355–1362.

Haboudane, D., Miller, J.R., Pattey, E., Zarco-Tejada, P.J., Strachan, I.B., 2004. Hyperspectral vegetation indices and novel algorithms for predicting green LAI of crop canopies: Modeling and validation in the context of precision agriculture. Remote Sens. Environ. 90, 337–352.

He, K., Zhang, X., Ren, S., Sun, J., 2016. Deep residual learning for image recognition. In : Proceedings of the IEEE conference on computer vision and pattern recognition. pp. 770–778.

Huete, A.R., 1988. A soil-adjusted vegetation index (SAVI). Remote Sens. Environ. 25 (3), 295–309.

Huete, A., Didan, K., Miura, T., Rodriguez, E.P., Gao, X., Ferreira, L.G., 2002. Overview of the radiometric and biophysical performance of the MODIS vegetation indices. Remote Sens. Environ. 83 (1–2), 195–213.

Ji, M., Yang, Y., Zheng, Y., Zhu, Q., Huang, M., Guo, Y., 2020. In-field automatic detection of maize tassels using computer vision. Inf. Process. Agric. 8 (1),, 87–95.

Jin, X., Li, Z., Feng, H., Ren, Z., Li, S., 2020a. Deep neural network algorithm for estimating maize biomass based on simulated Sentinel 2A vegetation indices and leaf area index. Crop J. 8 (1), 87–97.

Jin, X., Li, Z., Feng, H., Ren, Z., Li, S., 2020b. Estimation of maize yield by assimilating biomass and canopy cover derived from hyperspectral data into the AquaCrop model. Agric. Water Manag. 227, 105846.

Jin, X., Yang, W., Doonan, J.H., Atzberger, C., 2022. Crop phenotyping studies with application to crop monitoring. Crop J. 10 (5), 1221–1223.

Jordan, C.F., 1969. Derivation of leaf-area index from quality of light on the forest floor. Ecology 50, 663–666.

Kamboj, U., Guha, P., Mishra, S., 2021. Comparison of PLSR, MLR, SVM regression methods for determination of crude protein and carbohydrate content in stored wheat using near Infrared spectroscopy. Mater. Today: Proc. 48, 576–582.

Kimma, H., Kaiyu, G.B.C.J., Bin, P.B., Laura, F.G.C., Scott, C., Wilkinb, D., Sibo, W., Yaping, C., Carl, J.B.F., Jian, P., Yunan, L.G., 2020. Deriving high-spatiotemporal-resolution leaf area index for agroecosystems in the U.S. Corn Belt using Planet Labs CubeSat and STAIR fusion data. Remote Sens. Environ. 239, 111615.

Kumar, A., Desai, S.V., Balasubramanian, V.N., Rajalakshmi, P., Guo, W., Balaji Naik, B., Balram, M., Desai, U.B., 2021. Efficient maize tassel-detection method using UAV based remote sensing. Remote Sens. Appl.: Soc. Environ. 23, 100549.

Liang, L., Di, L., Zhang, L., Deng, M., Qin, Z., Zhao, S., Lin, H., 2015. Estimation of crop LAI using hyperspectral vegetation indices and a hybrid inversion method. Remote Sens. Environ. 165, 123–134.

Liu, S., Jin, X., Nie, C., Wang, S., Yu, X., Cheng, M., Shao, M., Wang, Z., Tuohuti, N., Bai, Y., Liu, Y., 2021. Estimating leaf area index using unmanned aerial vehicle data: shallow vs. deep machine learning algorithms. Plant Physiol. 187, 1551–1576.

Lu, H., Cao, Z., Xiao, Y., Li, Y., Zhu, Y., 2016. Region-based colour modelling for joint crop and maize tassel segmentation. Biosyst. Eng. 147, 139–150.

Lu, H., Cao, Z., Xiao, Y., Li, Y., Zhu, Y., 2015. Joint crop and tassel segmentation in the wild. In: 2015 Chinese Automation Congress (CAC). 2015 Chinese Automation Congress (CAC). IEEE, pp. 474–479.

Lu, H., Liu, L., Li, Y., Zhao, X., Wang, X., Cao, Z., 2021. TasselNETV3: explainable plant counting with guided upsampling and background suppression. IEEE Trans. Geosci. Remote Sens. 60, 1–15.

Lv, Z., Meng, R., Man, J., Zeng, L., Wang, M., Xu, B., Gao, R., Sun, R., Zhao, F., 2021. Modeling of winter wheat fAPAR by integrating Unmanned Aircraft Vehicle-based optical, structural and thermal measurement. Int. J. Appl. Earth Obs. Geoinf. 102, 102407.

Marcial-Pablo, M. D. J. U. ,Gonzalez-Sanchez, A., Jimenez-Jimenez, S. I. A. N., Ontiveros-Capurata, R. E., Ojeda-Bustamante, W, 2019 . Estimation of vegetation fraction using RGB and multispectral images from UAV. Int. J. Remote Sens. 40 (2): 420–438.

Metternicht, G., 2003. Vegetation indices derived from high-resolution airborne videography for precision crop management. Int. J. Remote Sens. 24 (14), 2855–2877.
Mirnezami, S.V., Srinivasan, S., Zhou, Y., Schnable, P.S., Ganapathysubramanian, B., 2021. Detection of the progression of anthesis in field-grown maize tassels: a case study. Plant Phenomics 2021, 4238701.
Morel, J., Bégué, A., Todoroff, P., Martiné, J., Lebourgeois, V., Petit, M., 2014. Coupling a sugarcane crop model with the remotely sensed time series of fIPAR to optimise the yield estimation. Eur. J. Agron. 61, 60–68.
Nguy-Robertson, A.L., Peng, Y., Gitelson, A.A., Arkebauer, T.J., Pimstein, A., Herrmann, I., Karnieli, A., Donald, R., C., and Bonfil, D. J., 2014. Estimating green LAI in four crops: potential of determining optimal spectral bands for a universal algorithm. Agric. For. Meteorol. 192–193, 140–148.
Ogunbadewa, and Yemi, E., 2012. Tracking seasonal changes in vegetation phenology with a SunScan canopy analyzer in northwestern England. For. Sci. Technol. 8, 161–172.
Pen Uelas, J., Filella, I., Lloret, P., Mun Oz, F., Vilajeliu, M., 1995. Reflectance assessment of mite effects on apple trees. Int. J. Remote Sens. 16, 2727–2733.
Putzenlechner, B., Marzahn, P., Kiese, R., Ludwig, R., Sanchez-Azofeifa, A., 2019. Assessing the variability and uncertainty of two-flux FAPAR measurements in a conifer-dominated forest. Agric. For. Meteorol. 264, 149–163.
Qi, J., Chehbouni, A., Huete, A.R., Kerr, Y.H., Sorooshian, S., 1994. A modified soil adjusted vegetation index. Remote Sens. Environ. 48 (2), 119–126.
Rondeaux, G., Steven, M., Baret, F., 1996. Optimization of soil-adjusted vegetation indices. Remote Sens. Environ. 55 (2), 95–107.
Ronneberger, O, Fischer, P, Brox, T., 2015. U-net: Convolutional networks for biomedical image segmentation 18 (pp), 234–241.
Rouse Jr., J.W., Haas, R.H., Schell, J.A., Deering, D.W., 1973. Monitoring the vernal advancement and retrogradation (green wave effect) of natural vegetation 01, 1–390. https://ntrs.nasa.gov/citations/19750020419.
Sandler, M., Howard, A., Zhu, M., Zhmoginov, A., Chen, L. C., 2018. Mobilenetv2: Inverted residuals and linear bottlenecks.In: Proceedings of the IEEE conference on computer vision and pattern recognition. pp: 4510-4520.
Shao, M., Nie, C., Cheng, M., Yu, X., Bai, Y., Ming, B., Song, H., Jin, X., 2022. Quantifying effect of tassels on near-ground maize canopy RGB images using deep learning segmentation algorithm. Precis. Agric. 23 (2), 400–418.
Tan, C., Samanta, A., Jin, X., Tong, L.u., Ma, C., Guo, W., Knyazikhin, Y., Myneni, R.B., 2013. Using hyperspectral vegetation indices to estimate the fraction of photosynthetically active radiation absorbed by corn canopies. Int. J. Remote Sens. 34 (24), 8789–8802.
Tanaka, S., Kawamura, K., Maki, M., Muramoto, Y., Yoshida, K., Akiyama, T., 2015. Spectral index for quantifying leaf area index of winter wheat by field hyperspectral measurements: a case study in Gifu Prefecture, Central Japan. Remote Sens. (Basel) 7, 5329–5346.
Tang, W., Zhang, Y., Zhang, D., et al., 2011. Corn tassel detection based on image processing. In: 2012 International Workshop on Image Processing and Optical Engineering, Vol. 8335. SPIE, pp. 123–129.
Tian, L., Wang, Z., Xue, B., Li, D., Zheng, H., Yao, X., Zhu, Y., Cao, W., Cheng, T., 2023. A disease-specific spectral index tracks Magnaporthe oryzae infection in paddy rice from ground to space. Remote Sens. Environ. 285, 113384.
Tucker, C.J., 1979. Red and photographic infrared linear combinations for monitoring vegetation. Remote Sens. Environ. 8 (2), 127–150.
Xie, Q., Dash, J., Huang, W., Peng, D., Qin, Q., Mortimer, H., Casa, R., Pignatti, S., Laneve, G., Pascucci, S., Dong, Y., Ye, H., 2018. Vegetation indices combining the red and red-edge spectral information for leaf area index retrieval. IEEE J. Sel. Top. Appl. Earth Obs. Remote Sens. 11 (5), 1482–1493.
Xu, X., Nie, C., Jin, X., Li, Z., Zhu, H., Xu, H., Wang, J., Zhao, Y.u., Feng, H., 2021b. A comprehensive yield evaluation indicator based on an improved fuzzy comprehensive evaluation method and hyperspectral data. Field Crop Res 270, 108204.
Xu, H., Zhang, X., Ye, Z.i., Jiang, L.i., Qiu, X., Tian, Y., Zhu, Y., Cao, W., 2021a. Machine learning approaches can reduce environmental data requirements for regional yield potential simulation. Eur. J. Agron. 129, 126335.
Xue, L., Cao, W., Luo, W., Dai, T., Zhu, Y., 2004. Monitoring leaf nitrogen status in rice with canopy spectral reflectance. Agron. J. 96 (1), 135–142.
Yang, B., Ma, J., Yao, X., Cao, W., Zhu, Y., 2021. Estimation of leaf nitrogen content in wheat based on fusion of spectral features and deep features from near infrared hyperspectral imagery. Sensors.21(2) 613.
Zarco-Tejada, P.J., Haboudane, D., Miller, J.R., Tremblay, N., Dextraze, L., 2002. Leaf Chlorophyll a+ b and canopy LAI estimation in crops using RT models and Hyperspectral Reflectance Imagery. http://hdl.handle.net/10261/10635.
Zeng, Y., Hao, D., Huete, A., Dechant, B., Berry, J., Chen, J.M., Joiner, J., Frankenberg, C., Bond-Lamberty, B., Ryu, Y., Xiao, J., Asrar, G.R., Chen, M., 2022. Optical vegetation indices for monitoring terrestrial ecosystems globally. Nat. Rev. Earth Environ. 3 (7), 477–493.
Zeng, L., Wardlow, B.D., Xiang, D., Hu, S., Li, D., 2020. A review of vegetation phenological metrics extraction using time-series, multispectral satellite data. Remote Sens. Environ. 237, 111511.